Vacuum 132 (2016) 1–4

Contents lists available at ScienceDirect

Vacuum

journal homepage: www.elsevier.com/locate/vacuum

Short communication

Large internal strains in very small iron oxide nanoparticles fabricated by spark discharge with electrodynamic acceleration of plasma jumpers

D.S. Portnov [a], I.V. Beketov [a], A. Larrañaga [b], A. Martínez-Amesti [b], G.V. Kurlyandskaya [c, d, *]

[a] Institute of Electrophysics, RAS, Urals Branch, 620016 Ekaterinburg, Russia
[b] SGIker, Servicios Generales de Investigación, UPV/EHU, 48080 Leioa, Spain
[c] Dpto. Electricidad y Electrónica, Universidad del País Vasco (UPV/EHU), 48940 Leioa, Spain
[d] Ural Federal University, 620002 Ekaterinburg, Russia

ARTICLE INFO

Article history:
Received 1 June 2016
Received in revised form
7 July 2016
Accepted 11 July 2016
Available online 14 July 2016

Keywords:
Spark discharge
Iron oxide nanoparticles
Internal strains

ABSTRACT

Iron oxide nanoparticles were fabricated by spark discharge method with electrodynamic acceleration of plasma jumpers. For different charging voltages of the capacitor from 8 to 15 kV the magnetite was the main phase represented by nanoparticles of 5–8 nm having *large internal strains* of the order of 25×10^{-3}.

1. Introduction

Biocompatible iron oxide nanoparticles (MNPs) were extensively studied with focus on biomedical applications [1]. For biological tasks, it is important to ensure spherical shape and a large single batch. One of the methods for MNP fabrication providing a high production rate is the electrophysical technique of the electric explosion of wire (EEW) [2]. It ensures fabrication of spherical MNPs with an average size of 20–100 nm. Another method is the laser target evaporation (LTE), which provides 10–50 nm MNPs [3]. There is a need to develop techniques for fabrication of MNPs with an average size below 10 nm. One of the candidates is the spark discharge method [4,5] for which researchers usually use microsecond generators with charging voltages not exceeding 5 kV. The distances between electrodes were typically below 3 mm and the energy stored by the capacitor around tens of mJ [5]. Small inter-electrode distances limited the volume in which the condensation of particles from the vapor phase took place, leading to the formation of rather large MNPs. We propose the approach for the diminishment of the MNPs size. Favorable situation arises for wider discharge gaps. In addition the original part of our approach is the use of electrodynamic acceleration of plasma jumpers, arising in the discharge gap. The directed motion of the plasma jumper gives an additional impetus to the evaporation products of the material of the electrode, which leads to a more rapid decrease in the concentration of vapors and the formation of small sized particles. In this work, we describe our experience in preparation of iron oxide MNPs with an average particle size below 10 nm by spark discharge with electrodynamic acceleration of plasma jumpers.

2. Experimental procedure

Iron oxide MNPs were obtained by spark discharge method. The procedure was carried out between two parallel disposed 10/50 mm cylindrical electrodes spaced at 9 mm (Fig. 1). Such configuration allowed realizing the electrodynamic acceleration of plasma inside the discharge gap. A single pulse 0.25 μF capacitor was used for the energy storage. The discharge of the capacitor through the gap was initiated by applying the trigger pulse to the control electrode located in the discharge gap at the repetition rate of the discharge pulses of 13 Hz and 3×10^4 number of pulses. The electrodes were made of low carbon steel.

* Corresponding author.Dpto. Electricidad y Electrónica, Universidad del País Vasco (UPV/EHU), 48940 Leioa, Spain.
E-mail address: galina@we.lc.ehu.es (G.V. Kurlyandskaya).

http://dx.doi.org/10.1016/j.vacuum.2016.07.015
0042-207X/

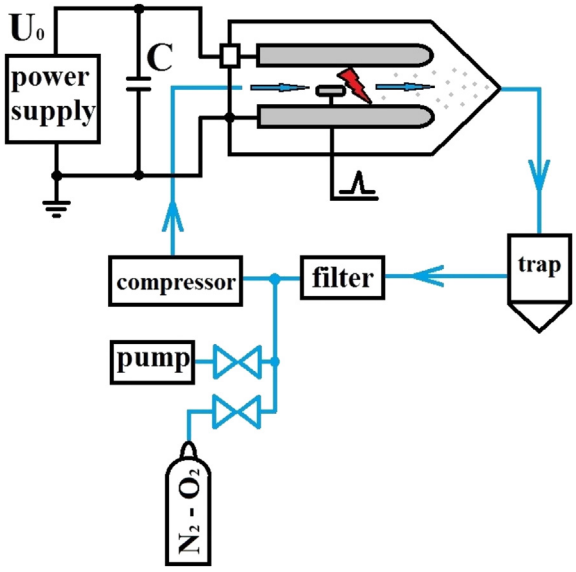

Fig. 1. Diagram of the installation: C – capacitor, U_o-charging voltage.

In order to insure the optimum material properties and to study the role of the technological parameters, the charge voltage of the capacitor U_o was varied from 8 to 15 kV. The discharge circuit was a low damped RLC circuit with average values of inductance of 450 nH and resistance of 0.3 Ohm. The MNPs were produced in N_2-20 vol %O_2 gas mixture at 0.12 MPa pressure and 70 l/min gas flow rate. The MNPs formed during the discharge passed through the trap, where micron sized particles were separated. The finest particles were collected by the porous stainless steel filter. The specific surface area (S_{sp}) defined by the low-temperature absorption of nitrogen was used for the evaluation of weighted average diameters (d_w) [2]. Transmission electron microscopy was performed by JEM 2100 microscope at 200 kV accelerating voltage.

X-ray powder diffraction (XRD) patterns were collected by a Philips X-Pert PRO automatic diffractometer operating at 40 kV and 40 mA, in theta-theta configuration, secondary monochromator with Cu-Kα radiation (λ = 1.5418 Å). A fixed divergence and anti-scattering slit giving a constant volume of sample illumination were used. Removal of the instrumental broadening was done collecting a pattern LaB_6 standard. Phase identification was evaluated using the Powder Diffraction File database. PANalytical X'Pert High Score program was used for indexing all the observed maxima. As a first step, the compounds were evaluated using the deconvolution of signals for the indication of the number of phases. This procedure was carried out using the peak-fit option of the WinPLOTR program without structural model. The simulated profiles were used to recalculate the starting unit cell parameters from the 2θ peak positions. After the identification, the diffraction data of the samples were fitted in all the cases by Rietveld method using the FULLPROF program [6,7].

3. Results and discussion

Table 1 shows the main synthesis conditions. The increase of the charging voltage of the capacitor and correspondingly of its stored energy $W_o = CU_o^2/2$ leads to the decrease of the S_{sp} and the increase of the specific output $m = M/N^*$ (M is the mass of the MNPs extracted from the filter and N^* is the number of the discharge pulses). With the increase of the energy stored in the capacitor, the amplitude of the discharge current increases leading to an intense evaporation of the material in the cathode/anode spots. The increase in the concentration of the metal vapors near the discharge zone increases both the size of the condensing particles and their amount. The erosion zone was clearly visible as an elongated area along the electrode surface. The length of the erosion zone is about 10 mm. The erosion zones of the both main electrodes (cathode and anode) were almost the same size, because during the discharge current flow their polarity was changed by several (4–5) times. The current changes its direction because of the low damped RLC circuit. The control electrode was subjected to erosion but to less extent as the discharge current flows via the main electrodes (anode and cathode).

The particle size distributions were obtained using TEM images. MNPs consist in a mixture of mainly of 1–18 nm small primary particles tending to be spherical and mixed agglomerates/aggregates with very few large particles of 20–90 nm (Fig. 2). In some cases, neck formation and elongated particles were observed. The increase of the energy stored in the capacitor shifts the particle size distribution toward the larger sizes and makes it wider (Fig. 3). Both small and large MNPs are homogeneous cubic (Fd3m) materials. TEM confirms the monocrystallinity of large MNPs. They are semitransparent and probably have a flattened shape. Crystallographic “twins” - a laminated structure manifesting the deformations appearing at the production - were observed in some large MNPs.

Fig. 4 shows the diffraction patterns of the S1 MNPs as an example. The MNPs contain fine and coarse magnetite and hematite (Table 1). In all cases, the amount of fine magnetite phase was above 80%. The grain size of the fine magnetite was decreased with the decrease of the charging voltage. The size of the crystallites of the other two phases is at least two orders of magnitude higher comparing with fine magnetite.

The most interesting result is the clearly observable high strain content for the fine magnetite. Concerning the micro-structural

Table 1
Processing conditions, specific surface, the particle size and XRD parameters. D_n - the average mean diameters for small and D_l - for large particles, H – hematite, FM – fine and CM – coarse magnetite.

Sample	U_o, kV	W_o, J	m, μg/pulse	S_{sp}, m^2/g	D_n, nm	D_l, nm	Phase	Size (XRD), nm	Maximum strain (XRD) × 10^{-3}	Content, wt.%
S1	15	28.1	2.0	106	6.8	45.2	H	–	5.4 ± 0.2	2.6 ± 1
							FM	8.4 ± 0.4	23.3 ± 0.6	87.6 ± 5
							CM	–	6.6 ± 0.4	9.8 ± 2
S2	12	18.0	1.4	123	6.2	34.4	H	–	6.5 ± 0.5	8.3 ± 2
							FM	7.3 ± 0.3	27.1 ± 0.9	81.6 ± 5
							CM	–	7.5 ± 0.4	10.1 ± 1
S3	8	8.0	0.5	147	5.3	31.7	H	–	5.8 ± 0.2	3.6 ± 1
							FM	5.2 ± 0.2	26.8 ± 0.2	86.8 ± 8
							CM	–	6.1 ± 0.2	9.6 ± 1

Note: The standard deviations appearing in the average apparent size and strain were calculated using the different reciprocal lattice directions. It is a measure of the degree of anisotropy, not of the estimated error. The broadening of reflections is resolution limited (sizes > 800 nm).